EasyChair Preprint

№ 14973

The Operating Diagram of an SIS Model in the Chemostat

Hayat Berhoune, Mustapha Lakrib and Tewfik Sari

September 21, 2024

The operating diagram of an SIS model in the chemostat

Hayat Berhoune[1,*], Mustapha Lakrib[2][0000−0002−5998−2067], and Tewfik Sari[3][0000−0002−6274−7826]

[1] LSDA, Abou Bekr Belkaid University, Tlemcen, Algeria
hayat.berhoune1@gmail.com
[2] LDM, Djillali Liabès University, Sidi Bel Abbès, Algeria
mustapha.lakrib@univ-sba.dz
[3] ITAP, University of Montpellier, INRAE, Institut Agro, Montpellier, France
tewfik.sari@inrae.fr

[*] Corresponding author

Abstract. This paper investigates the dynamics of a chemostat model incorporating two populations of one bacterial species: susceptible and virus-infected. Through the two operating parameters of the model, represented by the input concentration of the nutrient and the dilution rate of the chemostat, we analyze the existence and stability conditions of all possible equilibria, and then describe the operating diagram of the model, which is the bifurcation diagram giving its behavior with respect to those operating parameters, that visually depicts the various regions of stability of those equilibria. This diagram gives a better understanding of the complex interplay between bacterial populations growth, viral infection and environmental factors, in a controlled environment.

Keywords: Chemostat; SIS epidemic model; Operating diagram.

1 Introduction

The chemostat, which is a simple laboratory apparatus used for the continuous culture of microorganisms, was introduced by Novick and Szilard [1], and Monod [2]. For details on mathematical analysis of models of growth and competition in the chemostat, the reader is referred to [3–5]. In this work, we consider the following SIS model in the chemostat with general growth functions studied in [6]

$$\begin{cases} S' = (S^0 - S)D - \frac{1}{\eta_s} f_s(S)x_s - \frac{1}{\eta_i} f_i(S)x_i, \\ x_s' = (f_s(S) - D_s)\, x_s - \delta x_s x_i + \gamma x_i, \\ x_i' = (f_i(S) - D_i)\, x_i + \delta x_s x_i - \gamma x_i. \end{cases} \tag{1}$$

This model involves the competition for a single non-reproducing growth-limiting nutrient in a well-stirred chemostat in the presence of a virus. The concentration

of the nutrient at time t is denoted by $S(t)$. The bacteria species x is susceptible to attack by the virus, so it is divided into two subpopulations, susceptibles with concentration at time t denoted by $x_s(t)$ and infectives with concentration denoted by $x_i(t)$. The functions f_s and f_i represent the specific growth rates of the susceptible and infected bacteria, respectively. Since the virus requires a host to replicate, it is not included in the model explicitly. The disease dynamics are therefore modeled in the form of an SIS epidemic model. In system (1), S^0 denotes the input concentration of the nutrient, $D > 0$ is the dilution rate of the chemostat, and D_s and D_i are the removal rates of the bacteria, i.e. $D_s = D + \epsilon_s$ and $D_i = D + \epsilon_i$, denote the sum of the dilution D rate and the species-specific death rate. The parameters η_s and η_i are the growth yield coefficients, representing the conversion of nutrients to biomass. The rate of infection of susceptible bacteria in close proximity to infected bacteria is denoted by δ, and γ denotes the rate of elimination of virus. The parameters α_s and α_i denote the growth coefficients of susceptible and infected bacteria, respectively.

For the complete mathematical analysis of model (1), see reference [6].

Our objective in this work aligns with the methodology employed in [6], where we conducted a thorough examination of the long-term behavior of the system. The focus of our investigation centers on the critical operating parameters, specifically the input concentration of the nutrient S^0 and the dilution rate of the chemostat D. Our main goal is to construct a detailed operating diagram, which is a bifurcation diagram with respect to these critical operating parameters, that shows how the system behaves over a long time. As in [6], where the bifurcation diagram was used to illustrate the system's behavior as parameters vary, our study aims to provide a comprehensive portrayal of the chemostat's response to changes in S^0 and D.

The operating diagram is constructed in the book on the mathematical theory of the chemostat [4]. It is often constructed both in the biological literature [7–9] and in the mathematical modelling literature, as in the study of anaerobic digestion [10–14], microbial food-webs [15–18], inhibition and allelopathy [19–23], chemostats in series [24–26] and density dependent models [27–30].

The organization of this paper is as follows. In Section 2, we first present the assumptions made on the growth functions and the removal rates of model (1), and then the conditions for the existence and stability of its equilibria. In Section 3, we present operating diagrams. A conclusion is given in Section 4. Some auxiliary tables are reported in Appendix B, the parameter values used in simulations are provided in Appendix A and technical proofs are given in Appendix C.

2 Assumptions, notations and equilibria of the model

We use the following hypotheses on the growth functions and the removal rates of model (1)

(H1) $f_s(0) = f_i(0) = 0$ and, for all $S > 0$, $f_s'(S) > 0$ and $f_i'(S) > 0$.
(H2) For all $S \geq 0$, $f_s(S) \geq f_i(S)$.
(H3) $D_i \geq D_s$.

It is easy to verify that the positive cone is positively invariant and all solutions of (1) are positively bounded. We define the break-even concentrations λ_s and λ_i

$$\lambda_s = f_s^{-1}(D_s), \quad \lambda_i = f_i^{-1}(D_i). \tag{2}$$

When equation $f_s(S) = D_s$ or $f_i(S) = D_i$ has no solution, we put $\lambda_s = \infty$ or $\lambda_i = \infty$. We have $\lambda_s \leq \lambda_i$, see [6, Lemma 1].

In the sequel we will use the following notations a_3, where a_1, a_2 and a_3 are given by

$$\begin{aligned} X_s(S) &= \tfrac{\gamma + D_i - f_i(S)}{\delta}, \quad X_i(S) = \tfrac{f_s(S) - D_s}{D_i - f_i(S)} X_s(S), \\ F(S) &= \tfrac{1}{\eta_s} f_s(S) X_s(S) + \tfrac{1}{\eta_i} f_i(S) X_i(S). \end{aligned} \tag{3}$$

In the case $\lambda_s < \lambda_i$, we denote by $I := (\lambda_s, \lambda_i)$. The functions X_s, X_i and F are non negative on I, see [6, Remark 1].

2.1 Existence of equilibria

As shown in [6, Proposition 2], the existence of equilibria of system (1) are stated in Tables 5 and 6 in Appendix B, where

- The washout equilibrium is $E_0 = (S^0, 0, 0)$.
- The disease free equilibrium (DFE) is $E_1 = (\bar{S}, \bar{x}_s, 0)$, where

$$\bar{S} = \lambda_s, \qquad \bar{x}_s = \tfrac{D\eta_s}{D_s}(S^0 - \lambda_s), \tag{4}$$

with λ_s defined by (2).

- The coexistence equilibrium is $E_2 = (S^*, x_s^*, x_i^*)$, where

• in case $\lambda_s < \lambda_i$, S^* is a solution of equation

$$S^0 = G(S), \quad \text{with} \quad G(S) := S + \tfrac{1}{D} F(S), \tag{5}$$

where the function F is defined by (3), and x_s^*, x_i^* are given by

$$x_s^* = X_s(S^*), \qquad x_i^* = X_i(S^*), \tag{6}$$

where the functions X_s and X_i are defined by (3).

• in case $\lambda_s = \lambda_i$, we have $S^* = \lambda_s$ and

$$x_s^* = \tfrac{\gamma}{\delta}, \qquad x_i^* = \tfrac{\eta_i}{D_i}\left(D\left(S^0 - \lambda_s\right) - \tfrac{D_s \gamma}{\eta_s \delta}\right). \tag{7}$$

In the case $\lambda_s < \lambda_i$, we note that the number of positive equilibria depends on the number of solutions of the equation (5) belonging to I, which is related to the monotonicity or not of the function G. Therefore, equation

$$G'(S) = 0 \quad (\text{or, equivalently, } F'(S) = -D) \tag{8}$$

plays a major role in the discussion of the uniqueness or multiplicity of the positive equilibria, see Section 3.4.

2.2 Stability of equilibria

As shown in [6, Propositions 10 and 11], the local stability of equilibria E_0, E_1 and E_2 are given in Tables 5 and 6, where

- in case $\lambda_s < \lambda_i$, $c_4 = a_1 a_2 - a_3$, where a_1, a_2 and a_3 are given by

$$\begin{array}{l} a_1 = B + \gamma \frac{x_i^*}{x_s^*}, \\ a_2 = \frac{1}{\eta_s} f_s(S^*) x_s^* f_s'(S^*) + \frac{1}{\eta_i} f_i(S^*) x_i^* f_i'(S^*) + \delta x_i^* C + B \frac{\gamma x_i^*}{x_s^*}, \\ a_3 = \frac{1}{\eta_i} f_i(S^*) x_i^* \left(f_s'(S^*) \delta x_s^* + f_i'(S^*) \frac{\gamma x_i^*}{x_s^*} \right) + C \left(B \delta x_i^* - \frac{1}{\eta_s} f_s(S^*) x_i^* f_i'(S^*) \right) \end{array} \tag{9}$$

with $B = D + \frac{x_s^*}{\eta_s} f_s'(S^*) + \frac{x_i^*}{\eta_i} f_i'(S^*)$ and $C = \delta x_s^* - \gamma$.

- in case $\lambda_s = \lambda_i$, $c_4 = b_1 b_2 - b_3$, where b_1, b_2 and b_3 are given by

$$\begin{array}{l} b_1 = B + \delta x_i^*, \quad b_2 = \frac{D_s}{\eta_s} x_s^* f_s'(\lambda_s) + \frac{D_i}{\eta_i} x_i^* f_i'(\lambda_s) + B \delta x_i^*, \\ b_3 = \frac{D_i}{\eta_i} x_i^* \left(\gamma f_s'(\lambda_s) + f_i'(\lambda_s) \delta x_i^* \right), \end{array} \tag{10}$$

with $B = D + \frac{x_s^*}{\eta_s} f_s'(\lambda_s) + \frac{x_i^*}{\eta_i} f_i'(\lambda_s)$.

3 Operating diagrams

The operating diagram describes the asymptotic behavior of system (1) when the operating parameters, that are the substrate concentration S^0 and the dilution rate D, vary. In model (1), parameters such as specific death rates ϵ_s and ϵ_i, infection rate δ, virus elimination rate γ, growth yield coefficients η_s and η_i, and growth functions f_s and f_i, are biological parameters as they are organism- and substrate-dependent and are measurable through laboratory observations. In contrast, the parameters S^0 and D are called operating parameters since they are under the control of the experimenter.

In the sequel we assume that the biological parameters are fixed. The goal is then to identify regions within the operating diagram in the positive (S^0, D)-plan corresponding to distinct asymptotic behaviors.

Hereafter, break-even concentrations λ_s and λ_i in (2) are considered as functions of D

$$\lambda_s(D) = f_s^{-1}(D + \epsilon_s), \qquad \lambda_i(D) = f_i^{-1}(D + \epsilon_i). \tag{11}$$

We define the threshold λ_c depending on D

$$\lambda_c(D) = \lambda_s(D) + \frac{D + \epsilon_s}{\delta D \eta_s} \left(D + \epsilon_i - f_i(\lambda_s(D)) + \gamma \right). \tag{12}$$

When $\lambda_s = \lambda_i$, we have $D + \varepsilon_i - f_i(\lambda_s) = 0$ and the number (12) becomes

$$\lambda_c(D) = \lambda_s(D) + \frac{D + \epsilon_s}{\delta D \eta_s} \gamma. \tag{13}$$

Note that λ_s and λ_c are defined for $0 < D < f_s(+\infty) - \epsilon_s$, while λ_i is defined for $0 < D < f_i(+\infty) - \epsilon_i$. Note that λ_s and λ_i are increasing functions because f_s and f_i are.

3.1 Operating plan separation curves

As shown in [6, Proposition 2] (existence of E_0, E_1 and E_2) and [6, Proposition 10] (stability of E_0 and E_1), the Λ_1 and Λ_2 curves, defined in Table 4 in Appendix B, separate the positive (S^0, D)-plan into several regions where the system can have different asymptotic behaviour.

The Λ_3 curve in Table 4 corresponds to the condition of stability of E_2 given in [6, Proposition 11]. It is defined by equation $c_4(S^0, D) = 0$, where $c_4(S^0, D)$ is given by

$$c_4(S^0, D) = \begin{cases} (a_1 a_2 - a_3)(S^0, D) \text{ in case } \lambda_s < \lambda_i, \\ (b_1 b_2 - b_3)(S^0, D) \text{ in case } \lambda_s = \lambda_i, \end{cases} \tag{14}$$

where a_i, $i = 1, 2, 3$, are given by (9) and b_i, $i = 1, 2, 3$, are given by (10).

We have the following result.

Proposition 1. *The necessary and sufficient conditions of existence and local stability of equilibria E_0, E_1 and E_2 of (1) are summarized in Table 5, where $\lambda_s(D)$ and $\lambda_c(D)$ are defined by* (11) *and* (12)*, respectively, $S^*(S^0, D)$ is a solution of equation* (5) *and $c_4(S^0, D)$ is defined by* (14)*.*

Proof. This is a consequence of [6, Proposition 2] (existence of E_0, E_1 and E_2), [6, Proposition 10] (stability of E_0 and E_1) and [6, Proposition 11] (stability of E_2).

Remark 1. In both cases: (a) $\lambda_s(D) < \lambda_i(D)$ and $F'(S) > -D$ for any $S \in I(D) := (\lambda_s(D), \lambda_i(D))$, and (b) $\lambda_s(D) = \lambda_i(D)$, the conditions of existence and stability in Table 5 simplify as shown in Table 6.

3.2 Construction of the Λ_3 curve

The Λ_1 and Λ_2 curves, defined in Table 4, are graphs of functions while the Λ_3 curve is defined as the zero set of the c_4 function given by (14). We will see in the next two sections that these curves divide the positive operating plan into a number of regions where the system has an asymptotic behavior of a certain type. These regions together with the corresponding tables showing the asymptotic behaviour in each region are the operating diagram of the system.

Before constructing the operating diagram, our aim is to give a more precise description of the Λ_3 curve.

Case (a) : $\lambda_s(D) < \lambda_i(D)$ for all $D > 0$. Let

$$A_4(S, D) = (A_1 A_2 - A_3)(S, D), \tag{15}$$

where A_1, A_2 and A_3 are defined by $A_1 = B + \gamma \frac{X_i}{X_s}$, $A_2 = \frac{1}{\eta_s} f_s X_s f_s' + \frac{1}{\eta_i} f_i X_i f_i' + \delta X_i C + B \frac{\gamma X_i}{X_s}$ and $A_3 = \frac{1}{\eta_i} f_i X_i \left(f_s' \delta X_s + f_i' \frac{\gamma X_i}{X_s} \right) + C \left(B \delta X_i - \frac{1}{\eta_s} f_s X_i f_i' \right)$, with $B = D + \frac{X_s}{\eta_s} f_s' + \frac{X_i}{\eta_i} f_i'$ and $C = \delta X_s - \gamma$. Note that A_i are defined by the same formulas as a_i, see (9), where S^* is replaced by S and x_s^* and x_i^* are replaced by $X_s(S)$ and $X_i(S)$, defined by (3). Note also that they depend only

on the operating parameter D and not on the operating parameter S^0, unlike the quantities a_i in (14), which also depend on it. Using (6), we can write

$$a_i(S^0, D) = A_i(S^*(S^0, D), D), \quad i = 1, 2, 3, \tag{16}$$

where $S^*(S^0, D)$ is a solution of equation (5). This solution depends also on the operating parameter D since the G function depends on it.

To simplify the presentation, consider the case where there exists an interval $\mathcal{D}$ such that for $D \in \mathcal{D}$ there exist $S_1^H(D)$ and $S_2^H(D)$ such that $\lambda_s(D) < S_1^H(D) < S_2^H(D) < \lambda_i(D)$ and $A_4(S, D) < 0$ for $S \in (S_1^H(D), S_2^H(D))$, and positive outside this interval. We also assume that if $D \notin \mathcal{D}$ then $A_4(S, D) > 0$ for any $S \in I(D) = (\lambda_s(D), \lambda_i(D))$. The more general case where there exist more than two solutions $S_1^H(D)$ and $S_2^H(D)$, or where $\mathcal{D}$ is an union of intervals can be studied similarly. We have the following result.

Proposition 2. *The Λ_3 curve is such that*

$$\Lambda_3 = \{(D, S^0) : S^0 = \lambda_1^H(D)\} \cup \{(D, S^0) : S^0 = \lambda_2^H(D)\}, \tag{17}$$

where $\lambda_k^H(D)$, $k = 1, 2$, are defined by

$$\lambda_k^H(D) := G(S_k^H(D)) = S_k^H + \tfrac{1}{D} F\left(S_k^H\right), \quad k = 1, 2. \tag{18}$$

The numbers $\lambda_k^H(D)$ correspond to Hopf bifurcations of a positive equilibrium.

Proof. Using (16), $a_1 a_2 - a_3 = 0$ is equivalent to $A_1 A_2 - A_3 = 0$. The result follows from the fact that $S^*(D, S^0)$ is a solution of the equation $S^0 = G(S) := S + \frac{1}{D} F(S)$, see (5).

Case (b) : $\lambda_s(D) = \lambda_i(D)$ for all $D > 0$. Recall that E_2 exists (and is unique) if and only if $S^0 > \lambda_c(D)$ where the threshold $\lambda_c(D)$ is given by (13). In this case the condition of stability of E_2 is $c_4(S^0, D) > 0$, where c_4 is defined by (14), i.e. $c_4 = b_1 b_2 - b_3$, with b_i given by (10). Note that $b_1 b_2 - b_3$ is a polynomial of degree 3 in x_i^*, i.e. $b_1 b_2 - b_3 = b_4(x_i^*)$, where

$$b_4(X) := aX^3 + bX^2 + cX + d, \tag{19}$$

with $a = \frac{\delta^2}{\eta_i} f_i' + \frac{\delta}{\eta_i^2} f_i'^2$, $b = \delta^2 D + \frac{\delta\gamma}{\eta_s} f_s' + \frac{2\delta D}{\eta_i} f_i' + \frac{1}{\eta_i^2} f_i f_i'^2 + \frac{2\gamma}{\eta_s \eta_i} f_s' f_i'$, $c = \delta D^2 + \frac{\gamma}{\eta_s} f_s f_s' + \frac{D}{\eta_i} f_i f_i' + \frac{2\gamma D}{\eta_s} f_s' + \frac{\gamma}{\delta \eta_s \eta_i} (f_s + f_i) f_i' f_s' + \frac{\gamma^2}{\delta \eta_s^2} f_s'^2 - \frac{\gamma}{\eta_i} f_i f_s'$ and $d = \frac{D\gamma}{\delta \eta_s} f_s f_s' + \frac{\gamma^2}{\delta^2 \eta_s^2} f_s f_s'^2$.

The coefficients of $b_4(X)$ depend only on the operating parameter D, and not on S^0. This operating parameter appears in x_i^*, see (7). We need to study the positive roots of $b_4(X)$. We have the following result.

Lemma 1. *Let $\Delta = b^2 c^2 - 4ac^3 - 4b^3 d - 27a^2 d^2 + 18abcd$ be the discriminant of the polynomial b_4 given by (19). One and only one of the three following exclusive cases can occur.*

- *b_4 has no positive root if and only if $D \in Y_0$, where $Y_0 := \{D : \Delta < 0 \text{ or } c \geq 0\}$.*

– *b_4 has a positive double root if and only if $D \in Y_1$, where* $Y_1 := \{\ D : \Delta = 0 \text{ and } c < 0\}$.
– *b_4 has two positive distinct roots if and only if $D \in Y_2$, where* $Y_2 := \{\ D : \Delta > 0 \text{ and } c < 0\}$.

The proof is given in Appendix C.

From this lemma we can deduce now the sign of $c_4(S^0, D)$ defined by (14). Indeed, we have

Proposition 3. • *If $D \in Y_0$, then E_2 is locally asymptotically stable if and only if $S^0 > \lambda_c(D)$.*

• *If $D \in Y_2$, then E_2 is unstable if $\lambda_1^H(D) < S^0 < \lambda_2^H(D)$ and is locally asymptotically stable if $\lambda_c(D) < S^0 < \lambda_1^H(D)$ or $S^0 > \lambda_2^H(D)$, where $X_1^H(D) < X_2^H(D)$, the two positive real roots of $b_4(X)$, are defined by*

$$\lambda_k^H(D) = \lambda_c(D) + \tfrac{D_i}{\eta_i} X_k^H(D), \quad k = 1, 2. \tag{20}$$

The proof is given in Appendix C.

From this proposition we deduce that in the definition (17) of Λ_3 curve, $\lambda_k^H(D)$, $k = 1, 2$, are given by (20).

3.3 Operating diagram in case $\lambda_s = \lambda_i$

Here, we assume that $\lambda_s(D) = \lambda_i(D)$ for all $D > 0$. In this case, the positive equilibrium exists and is unique if and only if $S^0 > \lambda_c(D)$, where $\lambda_c(D)$ is given by (13). Using Remark 1, the necessary and sufficient conditions of existence and local stability of the equilibria E_0, E_1 and E_2 of (1) are summarized in Table 6, where $\lambda_s(D)$, $\lambda_c(D)$ and $c_4(S^0, D)$ are defined by (11), (13) and (14), respectively. Using Proposition 3, we know that the condition $c_4(S^0, D) < 0$ is equivalent to $\lambda_1^H(D) < S^0 < \lambda_2^H(D)$, where $\lambda_k^H(D)$ are defined by (20). Since

$$\lambda_s(D) < \lambda_c(D) < \lambda_1^H(D) < \lambda_2^H(D), \tag{21}$$

the curves Λ_1, Λ_2 and Λ_3 divide the positive (S^0, D)-plane in at most the four regions defined in Table 7 in Appendix B. Since $\lambda_c(D) > \lambda_s(D)$, for $D > 0$, the Λ_2 curve is located at the right of Λ_1 curve, so that the $\mathcal{J}_1$, $\mathcal{J}_2$ and $\mathcal{J}_3$ regions always exist (are not empty). However, the $\mathcal{J}_4$ region can be empty.

We can now give the asymptotic behaviour of (1) in each region of the operating diagram.

Proposition 4. *The asymptotic behaviours of equilibria of (1) are summarized in Table 1.*

The proof is given in Appendix C.

Table 1. Existence and stability of equilibria in the regions of the operating diagram in case of uniqueness of the positive equilibrium. The letter S (resp. U) means locally asymptotically stable (resp. unstable) equilibrium point. Absence of letter means that the equilibrium does not exist in the corresponding region.

Region	E_0	E_1	E_2
$\mathcal{J}_1$	S		
$\mathcal{J}_2$	U	S	
$\mathcal{J}_3$	U	U	S
$\mathcal{J}_4$	U	U	U

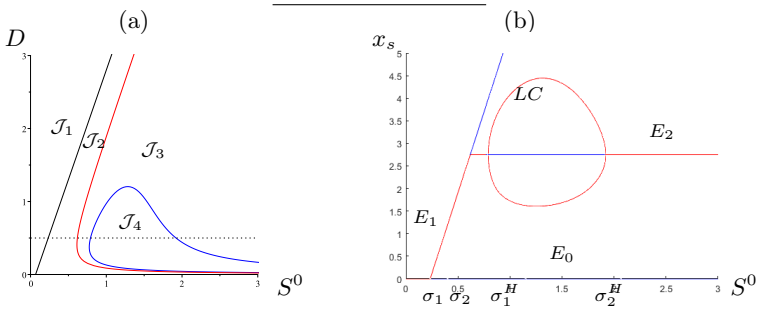

Fig. 1. (a) Operating diagram of (1) for the biological parameter values given in Table 3, line 4. The curves Λ_1 (in black), Λ_2 (in red) and Λ_3 (in blue) separate the operating plane into four regions $\mathcal{J}_1$, $\mathcal{J}_2$, $\mathcal{J}_3$ and $\mathcal{J}_4$. The existence and stability of equilibria are given in Table 1. (b) Bifurcation diagram corresponding to the line $D = 0.5$. We have $\sigma_1 \approx 0.23$, $\sigma_2 \approx 0.62$, $\sigma_1^H \approx 0.79$ and $\sigma_2^H \approx 1.92$. An equilibrium or a cycle is drawn in red when it is locally asymptotically stable and in blue when it is unstable.

The regions of the operating diagram are illustrated in Fig. 1(a) for the biological parameter values given in Table 3, line 4, in Appendix A. The sufficient condition of stability $\alpha_s + \alpha_i \geq \delta(\eta_s - \eta_i)$ in [6, Proposition 17, item (2)] is not satisfied: the region $\mathcal{J}_4$ is not empty. E_2 can lose its stability through a Hopf bifurcation, as depicted in Fig. 1(b). In this context, we show the bifurcation diagram of equilibria as S^0 varies and $D = 0.5$ is fixed. This bifurcation diagram was discussed in [6, Section 5].

Remark 2. The figures illustrating our results depict system (1) when the growth functions are linear: $f_s(S) = \alpha_s S$ and $f_i(S) = \alpha_i S$. The biological parameter values are given in Table 3. These values have no biological meaning. We chose them only to illustrate our findings and compare them with the results of [31] and [6].

3.4 Operating diagram in case $\lambda_s < \lambda_i$

We assume that $\lambda_s(D) < \lambda_i(D)$ for all $D > 0$, and consider two cases.

Uniqueness of the positive equilibrium This corresponds to the case where the equation (8) has no solution in $I = (\lambda_s, \lambda_i)$ (I depends on D). Then, the positive equilibrium exists if and only if $S^0 > \lambda_c(D)$. It is unique if it exists, and it is locally asymptotically stable if and only if $c_4(S^0, D) > 0$, see Table 6. The curves Λ_1, Λ_2 and Λ_3, defined in Table 4, separate the positive (S^0, D)-plane in at most four regions, given in Table 7.

We can give now the asymptotic behaviour of (1) in each region of the operating diagram.

Proposition 5. *Assume that $F'(S) > -D$ for any $S \in I$. The asymptotic behaviours of the equilibria of (1) are summarized in Table 1.*

Proof. The proof is the same as the proof of Proposition 4.

The regions of the operating diagram are illustrated in Fig. 2(a) in the case where the $\mathcal{J}_4$ region is empty. Indeed, since $\eta_s > \eta_i$ and $\alpha_s + \alpha_i > \delta(\eta_s - \eta_i)$ we deduce from [6, Proposition 17, item (2)] (see also [31, Theorem 3.4]) that the positive equilibrium E_2 is locally asymptotically stable and unique if it exists. Hence, using Proposition 5 we deduce that the asymptotic behavior of the equilibria is as in Table 1, where the regions of the operating diagram are depicted in Fig. 2(a). In Fig. 2(b) we show the bifurcation diagram of equilibria as S^0 varies and $D = 8$ is fixed. This bifurcation diagram was discussed in [6, Section 5].

The regions of the operating diagram are illustrated in Fig. 3 for the biological parameter values given Table 3, line 3. The sufficient condition of stability $\alpha_s + \alpha_i \geq \delta(\eta_s - \eta_i)$ in [6, Proposition 17, item (2)] is not satisfied, and we can see that $\mathcal{J}_4$ is not empty. Therefore E_2 can lose its stability through a Hopf bifurcation, see [6, Fig. 6] .

Multiplicity of positive equilibria Here the equation (8) has solutions S_k^{SN} in $I = (\lambda_s, \lambda_i)$, where $k = 1, 2, \cdots$, is an integer (S_k^{SN} and I depend on D). We define the following thresholds (depending on D) as relevant to the discussion of the existence and number of positive equilibria.

$$\lambda_k^{SN} := G(S_k^{SN}) = S_k^{SN} + \tfrac{1}{D} F\left(S_k^{SN}\right), \quad k = 1, 2, \cdots \tag{22}$$

The numbers λ_k^{SN} correspond to saddle-node bifurcations of the positive equilibria.

In this case, the multiplicity of positive equilibria can occur as shown in [6, Theorem 9]. The stability of a positive equilibrium depends on the signs of $F'(S^*) + D$ and c_4, see Table 5. Now, the curves Λ_k^{SN}, defined in Table 4, along which saddle-node bifurcations of positive equilibria occur, must be considered, see Table 4. It is not possible to give a general result as in Propositions 4 and 5 because the behavior of the system highly depends on the number of solutions $S_k^{SN}(D)$ of (8) which intervene in the definitions of the curves Λ_k^{SN}, see Table 4.

Let us show how this works for the biological parameter values used in [6, Figure 1(b)] for which we know that the multiplicity of positive equilibria can occur. As shown in [6, Appendix B.1], for these parameter values we can see that a critical value D_2 exists such that, if $D > D_2$, the equation (8) has only one solution $S_1^{SN}(D)$ in the interval I, and if $0 < D < D_2$, it has two solutions $S_2^{SN}(D) < S_1^{SN}(D)$ in the interval I, see Fig. 4. Moreover, a critical value $D_1 \in (0, D_2)$ exists such that

$$\begin{array}{ll} 0 < D < D_1 & \Longrightarrow \lambda_c(D) < \lambda_1^{SN}(D) < \lambda_2^{SN}(D), \\ D_1 < D < D_2 & \Longrightarrow \lambda_1^{SN}(D) < \lambda_c(D) < \lambda_2^{SN}(D), \\ D = D_1 & \Longrightarrow \lambda_1^{SN}(D_1) = \lambda_c(D_1), \\ D = D_2 & \Longrightarrow \lambda_2^{SN}(D_2) = \lambda_c(D_2). \end{array} \tag{23}$$

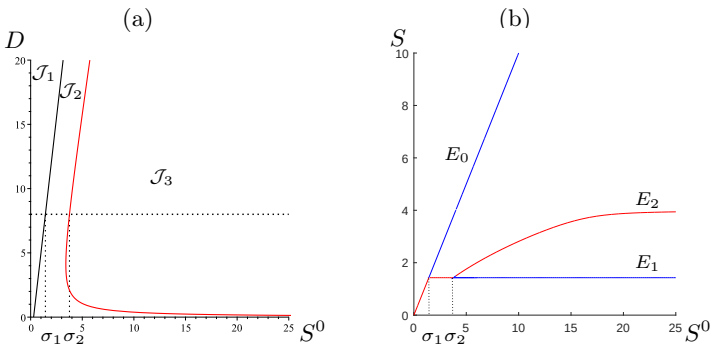

Fig. 2. (a) Operating diagram of (1) for parameters in Table 3, line 2. The curves Λ_1 (in black) and Λ_2 (in red) separate the operating plan into three regions $\mathcal{J}_1$, $\mathcal{J}_2$ and $\mathcal{J}_3$. The region $\mathcal{J}_4$ is empty. Equilibria details are given in Table 1. (b) Bifurcation diagram on $D = 8$ line, $\sigma_1 \approx 1.43$, $\sigma_2 \approx 3.76$. The color is red for stability and blue for instability.

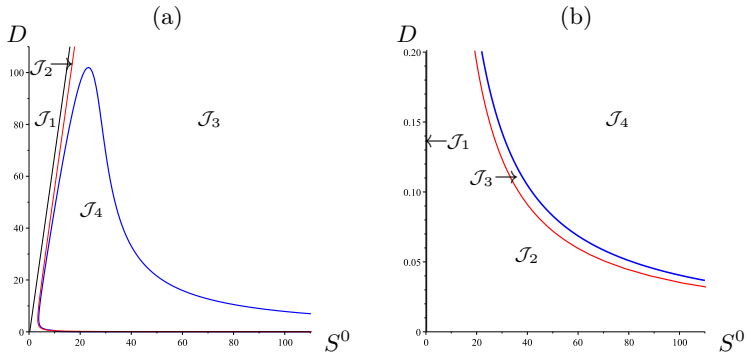

Fig. 3. Operating diagram of (1) for the biological parameter values given in Table 3, line 3. The existence and stability of equilibria are given in Table 1. (a) The curves Λ_1 (in black), Λ_2 (in red) and Λ_3 (in blue) separate the operating plan into four regions $\mathcal{J}_1$, $\mathcal{J}_2$, $\mathcal{J}_3$, and $\mathcal{J}_4$. (b) Magnification of the operating diagram for $0 < D < 0.2$, showing the regions near the S^0-axis.

From these properties we deduce that the curves Λ_1, Λ_2, Λ_1^{SN} and Λ_2^{SN} are as shown in Fig. 5. Hence, the Λ_1^{SN} curve separates the $\mathcal{J}_2$ region, located between Λ_1 and Λ_2 curves, in two sub-regions $\mathcal{J}_2^1$ and $\mathcal{J}_2^2$. Similarly, the Λ_1^{SN} and Λ_2^{SN} curves separate the $\mathcal{J}_3$ region, located at the right of Λ_2 curve, in three sub-regions $\mathcal{J}_3^1$, $\mathcal{J}_3^2$ and $\mathcal{J}_3^3$.

We can give now the asymptotic behaviour of the system in each region of the operating diagram.

Proposition 6. *Assume that the biological parameter values are given as in Fig. 5. In addition to washout equilibrium E_0 and the DFE E_1, the system can have three endemic equilibria E_2^k, $k = 1, 2, 3$. The asymptotic behaviours of the equilibria of (1) are summarized in Table 2.*

The proof is given in Appendix C.

Table 2. Existence and stability of equilibria in the regions of the operating diagram in case of multiplicity of positive equilibria. The letters S and U, and the absence of letter has the same meanings as in Table 1.

Region	E_0	E_1	E_2^1	E_2^2	E_2^3
$\mathcal{J}_1$	S				
$\mathcal{J}_2^1$	U	S			
$\mathcal{J}_2^2$	U	S		U	S
$\mathcal{J}_3^1$	U	U	S		
$\mathcal{J}_3^2$	U	U	S	U	S
$\mathcal{J}_3^3$	U	U			S

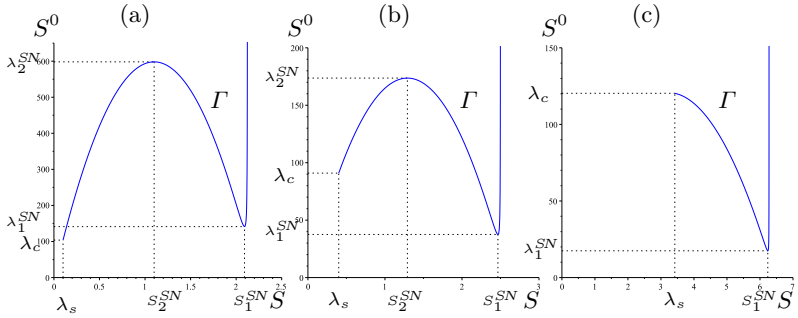

Fig. 4. The curve Γ as the graph of the function $S^0 = G(S)$ for the biological parameter values given in Table 3, line 5, for which $D_1 \approx 0.05993$ and $D_2 \approx 1.42359$. (a) The case $D = 0.04 < D_1$, for which $\lambda_c < \lambda_1^{SN} < \lambda_2^{SN}$. (b) The case $D = 0.8 \in (D_1, D_2)$, for which $\lambda_1^{SN} < \lambda_c < \lambda_2^{SN}$. (c) The case $D = 1.7 > D_2$, for which $\lambda_1^{SN} < \lambda_c$ and λ_2^{SN} does not exist.

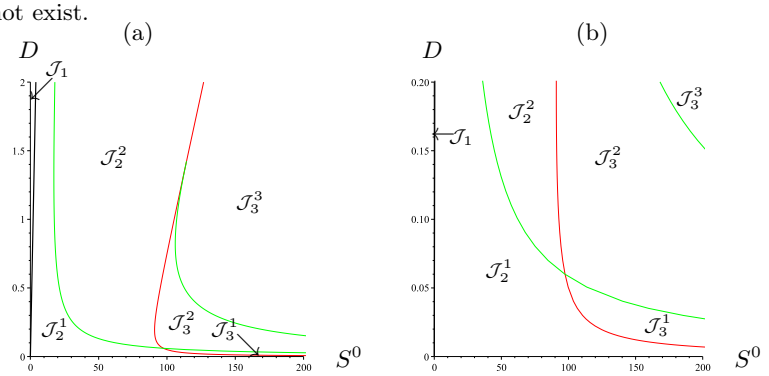

Fig. 5. Operating diagram of (1) for the biological parameter values used in Fig. 4. The existence and stability of equilibria are given in Table 2. (a) The curves Λ_1 (in black) and Λ_2 (in red) and the curves Λ_1^{SN} and Λ_2^{SN} (in green) separate the operating plan into six regions $\mathcal{J}_1$, $\mathcal{J}_2^1$, $\mathcal{J}_2^2$, $\mathcal{J}_3^1$, $\mathcal{J}_3^2$ and $\mathcal{J}_3^3$. The region $\mathcal{J}_4$ is empty. (b) Magnification of the operating diagram for $0 < D < 0.2$, showing the regions near the S^0-axis.

Remark 3. The system presents a bistability phenomenon. In $\mathcal{J}_2^2$ region, the DFE E_1 and the endemic equilibrium E_3^3 are both locally asymptotically stable. In $\mathcal{J}_3^2$ region, the endemic equilibria E_3^1 and E_3^3 are both locally asymptotically stable.

4 Conclusion

In this study, we examined the dynamics of an SIS (Susceptible- Infected- Susceptible) model with general growth functions, within a controlled environment, that is a chemostat. By introducing the operating diagram, which is a bifurcation diagram with respect to the control parameters, as a valuable tool for visualizing and predicting the behavior of the system, our analysis highlighted the importance of the two key parameters as control parameters: the dilution rate of the chemostat, D, and the input concentration of the nutrient, S^0. By analyzing this diagram, one can observe different zones of behavior based on varying combinations of D and S^0. This allows to predict the model's outcome and identify potential control strategies.

A Parameters used in numerical simulations

All the values of the parameters used in the numerical simulations are provided in Table 3 below.

Table 3. Biological parameter values used in the figures for the system (1) with linear growth functions $f_s(S) = \alpha_s S$ and $f_i(S) = \alpha_i S$.

Figure	ϵ_s	ϵ_i	η_s	η_i	α_s	α_i	δ	γ
2	2	12	10	5	7	5	0.7	0.2
3	2	192	55	0.5	7	6.5	2	0.01
1	0.2	0.2	10	0.01	3.0	3.0	2	5.5
4, 5	0.01	0.81	0.01	1	0.5	0.4	1	0.02

B Auxiliary tables

Table 4. The curves Λ_1, Λ_2, Λ_k^{SN}, $k = 1, 2, \cdots$ and Λ_3 of the operating diagram. λ_s, λ_c, λ_k^{SN} and $c_4(S^0, D)$ are defined by (11), (12), (22) and (14), respectively. The color column shows the corresponding colors of the curves in Figs. 1, 2(a), 3 and 5. Transcritical (TC) bifurcations of E_0 and E_1 occur on Λ_1. TC bifurcations of E_1 and E_2 occur on Λ_2. Saddle-node bifurcations (SN) of positive equilibria occur on Λ_k^{SN} and Hopf bifurcation of a positive equilibrium can occur on Λ_3.

Curve	Color	Bifurcation
$\Lambda_1 := \{(D, S^0) : S^0 = \lambda_s(D)\}$	Black	TC (E_0, E_1)
$\Lambda_2 := \{(D, S^0) : S^0 = \lambda_c(D)\}$	Red	TC (E_1, E_2)
$\Lambda_k^{SN} := \{(D, S^0) : S^0 = \lambda_k^{SN}(D)\}, \quad k = 1, 2, \cdots$	Green	SN (E_2^i, E_2^j)
$\Lambda_3 := \{(D, S^0) : c_4(S^0, D) = 0\}$	Blue	Hopf (E_2)

Table 5. Existence and local asymptotic stability of equilibria of (1) in case $\lambda_s < \lambda_i$. Here, λ_s, λ_c and c_4 are defined as in Table 4 and S^* is a solution of equation (5). Multiplicity of positive equilibria can occur.

Equilibrium	Existence	Stability
E_0	Always exists	$S^0 < \lambda_s(D)$
E_1	$S^0 > \lambda_s(D)$	$S^0 < \lambda_c(D)$
E_2	See [6, Theorem 9]	$F'(S^*(S^0, D)) > -D$ and $c_4(S^0, D) > 0$

Table 6. Existence and local asymptotic stability of equilibria of (1) in both cases: (a) $\lambda_s < \lambda_i$, when equation (8) has no solution in I, and (b) $\lambda_s = \lambda_i$. The numbers λ_s, λ_c and c_4 are defined as in Table 4. The positive equilibrium E_2 is unique if it exists.

Equilibrium	Existence	Stability
E_0	Always exists	$S^0 < \lambda_s(D)$
E_1	$S^0 > \lambda_s(D)$	$S^0 < \lambda_c(D)$
E_2	$S^0 > \lambda_c(D)$	$c_4(S^0, D) > 0$

Table 7. The regions of the operating diagram.

Region
$\mathcal{J}_1 := \{(S^0, D) : S^0 < \lambda_s(D)\}$
$\mathcal{J}_2 := \{(S^0, D) : \lambda_s(D) < S^0 < \lambda_c(D)\}$
$\mathcal{J}_3 := \{(S^0, D) : S^0 > \lambda_c(D) \text{ and } c_4(S^0, D) > 0\}$
$= \{(S^0, D) : \lambda_c(D) < S^0 < \lambda_1^H(D) \text{ or } S^0 > \lambda_2^H(D)\}$
$\mathcal{J}_4 := \{(S^0, D) : S^0 > \lambda_c(D) \text{ and } c_4(S^0, D) < 0\}$
$= \{(S^0, D) : \lambda_1^H(D) < S^0 < \lambda_2^H(D)\}$

C Proofs

Proof of Lemma 1

Since $a > 0$ and $d > 0$, the polynomial b_4 has at least one negative real root. If $\Delta < 0$, $b_4(X)$ has no other real root, so that it has no positive root. Since $b > 0$, if $c \geq 0$ the polynomial b_4 has no positive real root, because $b_4(X) > 0$ for any $X \geq 0$. Assume that $c < 0$. Since there are two changes of signs in the sequence of polynomial coefficients, the Descartes' rule of signs, asserts that the number of positive roots is 0 or 2. Since $bc < ad$, the Routh-Hurwitz condition is violated, so that the roots cannot be all of negative real part. Therefore, the polynomial has two positive real roots if, in addition, $\Delta \geq 0$.

Proof of Proposition 3

• If $D \in Y_0$ then, according to Lemma 1, b_4 has no positive real root, so that, it is always positive and E_2 is locally asymptotically stable whenever it exists, i.e. if $S^0 > \lambda_c(D)$. • If $D \in Y_2$, then, according to Lemma 1, b_4 has two positive real roots $X_1^H(D) < X_2^H(D)$. Hence c_4, defined by (14), is negative if $X_1^H(D) < x_i^* < X_2^H(D)$ and positive if $x_i^* < X_1^H(D)$ or $x_i^* > X_2^H(D)$. Therefore using the

definition (7) of x_i^*, we deduce that c_4 is negative if $\lambda_1^H(D) < S^0 < \lambda_2^H(D)$ and positive if $\lambda_c(D) < S^0 < \lambda_1^H(D)$ or $S^0 > \lambda_2^H(D)$, where $\lambda_1^H(D)$ and $\lambda_2^H(D)$ are defined by (20).

Proof of Proposition 4

According to Table 6, E_0 always exists and is locally asymptotically stable in the region to the left of curve Λ_1, which is region $\mathcal{J}_1$. In this region the equilibria E_1 and E_2 do not exist. On the other hand, E_1 exists in the regions to the right of curve Λ_1, that is to say in the regions $\mathcal{J}_2$, $\mathcal{J}_3$ and $\mathcal{J}_4$, and is locally asymptotically stable only in the region to the left of curve Λ_2, which is region $\mathcal{J}_2$. The positive equilibrium E_2 exists in the regions located at the right of curve Λ_2, that is to say regions $\mathcal{J}_3$ and $\mathcal{J}_4$ and is locally asymptotically stable in $\mathcal{J}_3$ and unstable in $\mathcal{J}_4$.

Proof of Proposition 6

According to Table 5, E_0 always exists and is locally asymptotically stable in the region to the left of the Λ_1 curve, which is region $\mathcal{J}_1$. In this region no other equilibrium exists. On the other hand, E_1 exists in the regions to the right of the Λ_1 curve, that is to say in the regions $\mathcal{J}_2^k$, $k = 1, 2$, and the regions $\mathcal{J}_3^k$, $k = 1, 2, 3$, and is locally asymptotically stable only in the regions to the left of the Λ_2 curve, which correspond to the regions $\mathcal{J}_2^k$, $k = 1, 2$.

The existence of positive equilibria is linked to the solutions of the equation (5). As shown in Fig. 1(b) in [6] and Fig. 4, we can have at most three positive equilibria, E_2^1, E_2^2 and E_2^3, associated to the solutions S_1^*, S_2^* and S_3^* of the equation (5), respectively. Here E_2^2 corresponds to the intersection with the decreasing branch of the Γ curve, which is the graph of the function $S^0 = G(S)$ in the (S, S^0)-plan, while E_2^1 and E_2^3 correspond to the intersections with the increasing branches of Γ, the first with the left branch and the second with the right branch. Note that if it exists, E_2^2 is unstable, because the condition $F'(S_2^*) < -D$ holds. On the contrary, if they exist, E_2^1 and E_2^3 are locally asymptotically stable, since the stability conditions $F'(S_1^*) > -D$ and $F'(S_3^*) > -D$ are satisfied. Moreover, as shown in item (3) of Proposition 17 in [6] (see also [31, Theorem 3.4]), since $\eta_i > \eta_s$ in Table 3, line 5 (corresponding to the biological parameter values used in Fig. 5), we have $c_4 > 0$. We deduce that E_2^1 and E_2^3 are locally asymptotically stable if they exist.

In the $\mathcal{J}_2^1$ region, we have $\lambda_s(D) < S^0 < \min\left(\lambda_1^{SN}(D), \lambda_c(D)\right)$, so there is no positive equilibrium point. In the $\mathcal{J}_2^2$ region, we have $\lambda_1^{SN}(D) < S^0 < \lambda_c(D)$, so that two positive equilibria E_2^2 and E_2^3 exist. The first is unstable and the second is locally asymptotically stable. In the $\mathcal{J}_3^2$ region, we have $\max\left(\lambda_1^{SN}(D), \lambda_c(D)\right) < S_0 < \lambda_2^{SN}(D)$, so that three positive equilibria E_2^1, E_2^2 and E_2^3 exist. The first and third are locally asymptotically stable and the second is unstable. The proofs for $\mathcal{J}_3^1$ and $\mathcal{J}_3^3$ regions are similar and left to the reader.

Acknowledgments

We thank the support of the Directorate General for Scientific Research and Technological Development (DGSRTD), Ministry of Higher Education and Scientific Research, Algeria, the Euro-Mediterranean research network TREASURE (https://www.inrae.fr/treasure) and the Algerian-Tunisian research project DGRSDT/DGRS: Mathematical ecology, modeling and optimization of depollution bioprocesses.

References

1. Novick, A., Szilard, L.: Description of the chemostat. Science **112**(2920), 715-716 (1950). https://doi.org/10.1126/science.112.2920.7
2. Monod, J.: La technique de culture continue: théorie et applications. Ann. Inst. Pasteur **79**, 390–410 (1950). https://doi.org/10.1016/B978-0-12-460482-7.50023-3
3. Monod, J. . Recherches sur la croissance des cultures bacteriennes. Hermann, Paris (1958)
4. Harmand, J., Lobry, C., Rapaport, A., Sari, T.: The Chemostat: Mathematical Theory of Microorganism Cultures. Wiley-ISTE (2017). http://doi.org/10.1002/9781119437215
5. Smith, H. L., Waltman, P.: The theory of the chemostat: dynamics of microbial competition. Cambridge University Press (1995)
6. Berhoune, H., Bar, B., Lakrib, M., Sari, T.: An SIS model in the Chemostat. (2023). https://hal.science/hal-04293111v1
7. Jost, J. L., Drake, J. F., Fredrickson, A. G., Tsuchiya, H. M.: Interactions of Tetrahymena pyriformis, Escherichia coli, Azotobacter vinelandii, and glucose in a minimal medium. J. Bacteriol. **113**(2), 834-840 (1973). http://doi.org/10.1128/jb.113.2.834-840.1973
8. Lenski, R. E., Hattingh, S. E.: Coexistence of two competitors on one resource and one inhibitor: a chemostat model based on bacteria and antibiotics. J. Theoret. Biol. **122**(1), 83-93 (1986). http://doi.org/10.1016/s0022-5193(86)80226-0
9. Xu, A., Dolfing, J., Curtis, TP, Montague, G., Martin, E.: Maintenance affects the stability of a two-tiered microbial 'food chain'? J. Theoret. Biol. **276**(1), 35-41 (2011). https://doi.org/10.1016/j.jtbi.2011.01.026
10. Khedim, Z., Benyahia, B., Cherki, B., Sari, T., Harmand, J.: Effect of control parameters on biogas production during the anaerobic digestion of protein-rich substrates. Appl. Math. Modelling **61**, 351-376 (2018). https://doi.org/10.1016/j.apm.2018.04.020
11. Sari, T.: Best operating conditions for biogas production in some simple anaerobic digestion models. Processes **10**(2), 258 (2022). https://doi.org/10.3390/pr10020258
12. Sari, T., Benyahia, B.: The operating diagram for a two-step anaerobic digestion model. Nonlinear Dyn. **105**, 2711-2737 (2021). https://doi.org/10.1007/s11071-021-06722-7
13. Weedermann, M., Wolkowicz, G. S. K., Sasara, J.: Optimal biogas production in a model for anaerobic digestion. Nonlinear Dyn. **81**, 1097-1112 (2015). https://doi.org/10.1007/s11071-015-2051-z
14. Sari, T., Harmand, J.: A model of a syntrophic relationship between two microbial species in a chemostat including maintenance. Math. Biosci. **275**, 1-9 (2016). https://doi.org/10.1016/j.mbs.2016.02.008

15. Daoud, Y., Abdellatif, N., Sari, T., Harmand, J.: Steady state analysis of a syntrophic model: The effect of a new input substrate concentration. Math. Model. Nat. Phenom. **13**(3), 31 (2018). https://doi.org/10.1051/mmnp/2018037
16. Fekih-Salem, R., Daoud, Y., Abdellatif, N., Sari, T.: A mathematical model of anaerobic digestion with syntrophic relationship, substrate inhibition, and distinct removal rates. SIAM J. Appl. Dyn. Syst. **20**(3), 1621-1654 (2021). https://doi.org/10.1137/20M1376480
17. Nouaoura, S., Fekih-Salem, R., Abdellatif, N., Sari, T.: Operating diagrams for a three-tiered microbial food web in the chemostat. J. Math. Biol., **85**(5), 44 (2022). https://doi.org/10.1007/s00285-022-01812-5
18. Sari, T., Wade, M. J.: Generalised approach to modelling a three-tiered microbial food-web. Math. biosci. **291**, 21-37 (2017). https://doi.org/10.1016/j.mbs.2017.07.005
19. Bar, B., Sari, T.: The operating diagram for a model of competition in a chemostat with an external lethal inhibitor. Discrete Contin. Dyn. Syst. B **25**(6), 2093-2120 (2020). https://doi.org/10.3934/dcdsb.2019203
20. Dellal M., Bar B.: Global analysis of a model of competition in the chemostat with internal inhibitor. Discrete Contin. Dyn. Syst. B **26**(2), 1129–1148 (2021). https://doi.org/10.3934/dcdsb.2020156
21. Dellal, M., Bar, B., Lakrib, M.: A competition model in the chemostat with allelopathy and substrate inhibition. Discrete Contin. Dyn. Syst. B **27**(4), 2025-2050 (2022). https://doi.org/10.3934/dcdsb.2021120
22. Dellal, M., Lakrib, M.: The operating diagram of a model of two competitors in a chemostat with an external inhibitor. Math. biosci. **302**, 27-45 (2018). https://doi.org/10.1016/j.mbs.2018.05.004
23. Zitouni, N. E. H., Dellal, M., Lakrib, M.: Substrate inhibition can produce coexistence and limit cycles in the chemostat model with allelopathy. J. Math. Biol. **87**(1), 7 (2023). https://doi.org/10.1007/s00285-023-01943-3
24. Dali-Youcef, M., Rapaport, A., Sari, T.: Study of performance criteria of serial configuration of two chemostats. Math. Biosci. Eng. **17**(6), 6278-6309 (2023). https://doi.org/10.3934/mbe.2020332
25. Dali-Youcef, M., Rapaport, A., Sari, T.: Performance study of two serial interconnected chemostats with mortality. Bul. Math. Biol. **84**(10), 1-10 (2022). https://doi.org/10.1007/s11538-022-01068-6
26. Dali-Youcef, M., Sari, T.: The productivity of two serial chemostats. Int. J. Biomath. **16**(06), 2250113 (2023). https://doi.org/10.1142/S1793524522501133
27. Abdellatif, N., Fekih-Salem, R., Sari, T.: Competition for a single resource and coexistence of several species in the chemostat. Math. Biosci. Eng. **13**(4), 631-652 (2016). https://doi.org/10.3934/mbe.2016012
28. Fekih-Salem, R., Lobry, C., Sari, T.: A density-dependent model of competition for one resource in the chemostat. Math. biosci. **286**, 104-122 (2017). https://doi.org/10.1016/j.mbs.2017.02.007
29. Mtar, T., Fekih-Salem, R., Sari, T.: Interspecific density-dependent model of predator–prey relationship in the chemostat. Int. J. Biomath. **14**(01), 2050086 (2021). https://doi.org/10.1142/S1793524520500862
30. Mtar, T., Fekih-Salem, R., Sari, T.: Mortality can produce limit cycles in density-dependent models with a predator-prey relationship. Discrete Contin. Dyn. Syst. B **27**(12), 7445-7467 (2022). https://doi.org/10.3934/dcdsb.2022049
31. Northcott, K., Imran, M., Wolkowicz, G. S. K.: Competition in the presence of a virus in an aquatic system: an SIS model in the chemostat. J. Math. Biol. **64**, 1043-1086 (2012). https://doi.org/10.1007/s00285-011-0439-z